



AFRL-RI-RS-TR-2015-013

**HYBRID CIRCUIT QUANTUM ELECTRODYNAMICS:
COUPLING A SINGLE SILICON SPIN QUBIT TO A PHOTON**

PRINCETON UNIVERSITY

JANUARY 2015

FINAL TECHNICAL REPORT

APPROVED FOR PUBLIC RELEASE; DISTRIBUTION UNLIMITED

STINFO COPY

**AIR FORCE RESEARCH LABORATORY
INFORMATION DIRECTORATE**

NOTICE AND SIGNATURE PAGE

Using Government drawings, specifications, or other data included in this document for any purpose other than Government procurement does not in any way obligate the U.S. Government. The fact that the Government formulated or supplied the drawings, specifications, or other data does not license the holder or any other person or corporation; or convey any rights or permission to manufacture, use, or sell any patented invention that may relate to them.

This report is the result of contracted fundamental research deemed exempt from public affairs security and policy review in accordance with SAF/AQR memorandum dated 10 Dec 08 and AFRL/CA policy clarification memorandum dated 16 Jan 09. This report is available to the general public, including foreign nationals. Copies may be obtained from the Defense Technical Information Center (DTIC) (<http://www.dtic.mil>).

AFRL-RI-RS-TR-2015-013 HAS BEEN REVIEWED AND IS APPROVED FOR PUBLICATION IN ACCORDANCE WITH ASSIGNED DISTRIBUTION STATEMENT.

FOR THE DIRECTOR:

/ S /

PAUL ALSING
Work Unit Manager

/ S /

MARK LINDERMAN
Technical Advisor, Computing &
Communications Division
Information Directorate

This report is published in the interest of scientific and technical information exchange, and its publication does not constitute the Government's approval or disapproval of its ideas or findings.

REPORT DOCUMENTATION PAGE

Form Approved
OMB No. 0704-0188

The public reporting burden for this collection of information is estimated to average 1 hour per response, including the time for reviewing instructions, searching existing data sources, gathering and maintaining the data needed, and completing and reviewing the collection of information. Send comments regarding this burden estimate or any other aspect of this collection of information, including suggestions for reducing this burden, to Department of Defense, Washington Headquarters Services, Directorate for Information Operations and Reports (0704-0188), 1215 Jefferson Davis Highway, Suite 1204, Arlington, VA 22202-4302. Respondents should be aware that notwithstanding any other provision of law, no person shall be subject to any penalty for failing to comply with a collection of information if it does not display a currently valid OMB control number.

PLEASE DO NOT RETURN YOUR FORM TO THE ABOVE ADDRESS.

1. REPORT DATE (DD-MM-YYYY) JANUARY 2015			2. REPORT TYPE FINAL TECHNICAL REPORT		3. DATES COVERED (From - To) JUN 2012 – MAY 2014	
4. TITLE AND SUBTITLE HYBRID CIRCUIT QUANTUM ELECTRODYNAMICS: COUPLING A SINGLE SILICON SPIN QUBIT TO A PHOTON					5a. CONTRACT NUMBER FA8750-12-2-0296	
					5b. GRANT NUMBER N/A	
					5c. PROGRAM ELEMENT NUMBER	
6. AUTHOR(S) Jason R. Petta					5d. PROJECT NUMBER QUEST	
					5e. TASK NUMBER PR	
					5f. WORK UNIT NUMBER IN	
7. PERFORMING ORGANIZATION NAME(S) AND ADDRESS(ES) Princeton University, Jadwin Hall Department of Physics Princeton, NJ 08544					8. PERFORMING ORGANIZATION REPORT NUMBER	
9. SPONSORING/MONITORING AGENCY NAME(S) AND ADDRESS(ES) Air Force Research Laboratory/RITA 525 Brooks Road Rome NY 13441-4505					10. SPONSOR/MONITOR'S ACRONYM(S) AFRL/RI	
					11. SPONSOR/MONITOR'S REPORT NUMBER AFRL-RI-RS-TR-2015-013	
12. DISTRIBUTION AVAILABILITY STATEMENT Approved for Public Release; Distribution Unlimited. This report is the result of contracted fundamental research deemed exempt from public affairs security and policy review in accordance with SAF/AQR memorandum dated 10 Dec 08 and AFRL/CA policy clarification memorandum dated 16 Jan 09.						
13. SUPPLEMENTARY NOTES						
14. ABSTRACT The purpose of this research program was to develop a device architecture that is capable of coherently coupling two silicon spin qubits via the electromagnetic field of superconducting resonator. Single Electron spins can be efficiently coupled using the exchange interaction, but the strength of exchange falls of very quickly as a function of the distance separating the two electron spins. Cavity based coupling schemes have recently emerged as a robust tool for coupling superconducting quantum bits. The main goal of this research program was to make the first steps toward combing elements of the superconducting and semiconductor qubit architectures.						
15. SUBJECT TERMS Quantum Computing, Quantum Hybrid Circuits, Quantum Electrodynamics, Coupling a Single Silicon Spin Qubit to a Photon						
16. SECURITY CLASSIFICATION OF:			17. LIMITATION OF ABSTRACT UU	18. NUMBER OF PAGES 25	19a. NAME OF RESPONSIBLE PERSON PAUL ALSING	
a. REPORT U	b. ABSTRACT U	c. THIS PAGE U			19b. TELEPHONE NUMBER (Include area code) N/A	

TABLE OF CONTENTS

LIST OF FIGURES	ii
1.0 SUMMARY	1
2.0 INTRODUCTION	1
3.0 METHODS, ASSUMPTIONS AND PROCEDURES	3
3.1 Superconducting resonator.....	3
3.2 Double quantum dot.....	4
3.3 Micromagnet.....	4
3.4 Discussion of other possible spin coupling approaches.....	4
4.0 RESULTS AND DISCUSSION	6
4.1 Development of high quality factor superconducting resonators on Si/SiGe two-dimensional electron gas substrates.....	6
4.2 Resonator fabrication.....	6
4.3 Simulations to determine the effect of the substrate resistivity on the resonator quality factor	8
4.4 Testing of Nb resonators on high-resistivity Si.....	9
4.5 Testing of Nb resonators on high-resistivity Si with a SiGe relaxed buffer substrate	11
4.6 Testing of Nb resonators on high-resistivity Si with Si _{0.7} Ge _{0.3} relaxed buffer layers and a dc contact for electrical coupling to a triple quantum dot.....	12
4.7 Testing of Nb resonators on high-resistivity Si with Si _{0.7} Ge _{0.3} relaxed buffer with a gold contact for coupling to triple quantum dot and gold gates.....	14
4.8 Summary of resonator optimizations and possible further optimizations.....	16
4.9 Testing of Hall bars on low-resistivity Si with a Si/SiGe heterostructure	16
4.10 Development of accumulation only gate architecture.....	17
5.0 CONCLUSIONS.....	18
6.0 REFERENCES	19
7.0 LIST OF SYMBOLS, ABBREVIATIONS, AND ACRONYMS.....	20

LIST OF FIGURES

Figure 1: Superconducting resonator architecture	2
Figure 2: Fault-tolerant spin-based quantum computer architecture proposed by Taylor <i>et al.</i>	5
Figure 3: Spin chain approach for the transfer of quantum information.....	5
Figure 4: Transmission versus frequency for the resonator on low-resistivity Si with a Si/SiGe heterostructure at 4.2 K.....	7
Figure 5: Transmission versus frequency for the resonator on low-resistivity Si and Ar destructed SiGe heterostructure at 4.2 K.....	7
Figure 6: Electric field simulation of a superconducting resonator	8
Figure 7: Optical micrograph of the resonator’s center pin	9
Figure 8: Design of the resonator coupling capacitor	9
Figure 9: Transmission versus frequency for Design 1 on bare high-resistivity Si at 4.2 K	10
Figure 10: Transmission versus frequency for Design 1 on bare high-resistivity Si at 8 mK	10
Figure 11: Transmission versus frequency for Design 1 on high-resistivity Si with a SiGe relaxed buffer at 4.2 K.....	11
Figure 12: Transmission versus frequency for Design 1 on high-resistivity Si with a SiGe relaxed buffer at 10 mK.....	12
Figure 13: Transmission versus frequency for design A0 at 4.2 K.....	13
Figure 14: Transmission versus frequency for design B0 at 4.2 K with its spiral inductor floating.....	13
Figure 15: Transmission versus frequency for design A0 at 10 mK.....	14
Figure 16: Transmission versus frequency at 4.2 K for design A0 with thick gold gates added.....	14
Figure 17: Transmission versus frequency at 10 mK for design A0 with thick gold gates added.....	15
Figure 18: Quality factor versus approximate number of photons in the cavity for design A0 with thick gold gates	15
Figure 19: Hall bar testing	17
Figure 20: SEM image of an “accumulation only” double quantum dot.....	17
Figure 21: Few electron charge stability diagram.....	18

1.0 SUMMARY

The purpose of this research program is develop a device architecture that is capable of coherently coupling two silicon spin qubits via the electromagnetic field of a superconducting resonator. Single electron spins can be efficiently coupled using the exchange interaction, but the strength of exchange falls off very quickly as a function of the distance separating the two electron spins. Cavity based coupling schemes have recently emerged as a robust tool for coupling superconducting quantum bits. The main goal of this research program is to make the first steps toward combining elements of the superconducting and semiconductor qubit architectures.

2.0 INTRODUCTION

Universal quantum computing with electron spins requires single spin control and two qubit interactions. It is possible to couple two electron spins efficiently using the exchange interaction. Since the exchange interaction is based on electron tunneling, the exchange gate is a nearest neighbor interaction, which cannot be used to couple two spins separated by a large distance. In a realistic computing architecture, it is desirable to be able to couple quantum bits beyond nearest neighbor. There are at least two approaches that can be pursued to address this problem. The first is based on a Heisenberg spin chain (1-3). A linear array of exchange coupled electron spins can in theory be used to transfer quantum information over a large distance. This method requires the fabrication of such a spin chain, as well as control over the tunnel coupling between each spin site. A second approach follows a theme that has been very successfully employed by the superconducting qubit community. In this approach, quantum bits are coupled to a high quality factor superconducting resonator (4-6). The superconducting resonator supports electric fields that couple strongly to the superconducting bits, serving as a “quantum bus” that can be used to entangle spatially separated qubits. Superconducting qubits have demonstrated rapid scaling from one to four qubits using the quantum bus architecture (6, 7). A key figure of merit is the number of Rabi oscillations the system can support, $n_{\text{rabi}}=2g^2/(\kappa+\gamma)$. Here g is the charge coupling strength, κ is the cavity decay rate, and γ is the qubit decay rate. Present superconducting technologies support n_{rabi} of 500 (5, 8).

The purpose of the proposed research program is to leverage the successes that have been obtained in the superconducting community and apply them to spin qubits. Spin qubits can be coupled at short length scales using the exchange interaction, which is based on electron tunneling (9). There have been attempts to couple two GaAs singlet-triplet qubits via a capacitive interaction, but the efforts have been hampered by short dephasing times and $1/f$ charge noise. Our approach is to couple two spin qubits to the electric field of the cavity using spin-orbit coupling that is generated by a magnetic field gradient.

Direct coupling of a single spin to the magnetic field of a microwave cavity is far too small to allow coherent exchange of quantum information from the qubit to the cavity. Due to the small magnetic moment of the electron and the small magnetic field generated by the cavity ($B \sim 1$ nT), the effective coupling rate is on the order of 10 Hz. An alternative approach is to couple the charge of a single electron to the electric field of the cavity and then use spin-orbit interactions to couple the spin to position. This is effectively a second-order coupling process, but it can yield spin-electric coupling rates that are much faster than the 10 Hz interaction rate obtained by coupling a single spin to the magnetic field of the cavity.

The device concept for this work is based on a circuit quantum electrodynamics (cQED) sample geometry developed by the Princeton group to study spin-cavity coupling in InAs nanowires. The sample, shown in Fig. 1, couples an InAs spin-orbit qubit to a high quality factor superconducting resonator. The superconducting resonator is fabricated by depositing 100 nm of Nb and then selectively etching portions away using photolithography and a wet chemical etch. The resonator has an oscillation frequency of ~ 6 GHz and results in a large electric field amplitude of 0.2 V/m (4, 6). It is this electric field that couples to the charge trapped in the InAs nanowire quantum dot.

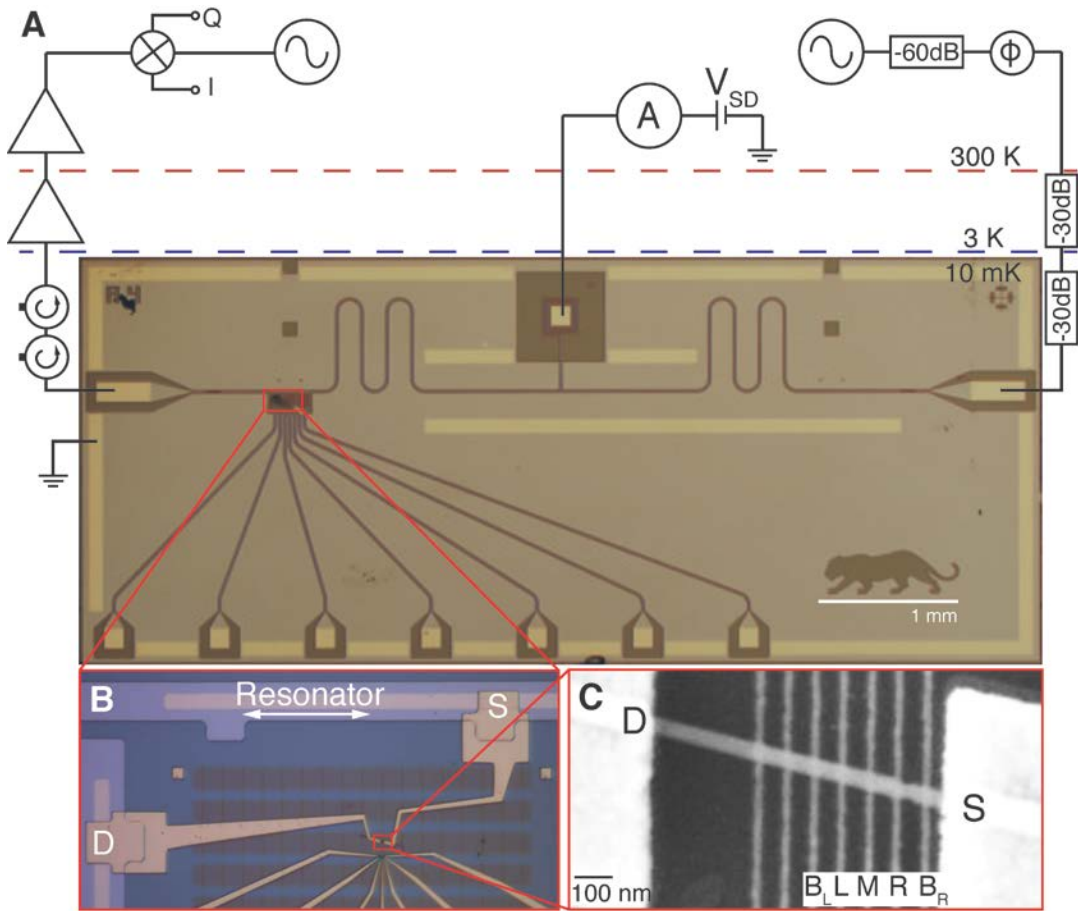


Figure 1. Superconducting resonator architecture. A) A Nb stripline resonator supports a 6 GHz resonant frequency. B) We couple a single InAs nanowire double quantum dot to the resonator. Charge trapped in the double quantum dot couples to the electric field of the cavity. Spin-orbit interactions in InAs couple the spin of the electron to its orbital motion. C) Scanning electron microscope image of the nanowire double quantum dot. Bottom gates define the confinement potential. The electric field of the resonator is dropped along the length of the nanowire, resulting in a large coupling rate of 30 MHz.

A double quantum dot is defined in a bottom gated InAs nanowire. We couple a *single* spin qubit to the resonator in this experiment. A single charge trapped in the double quantum dot can tunnel back and forth, resulting in a dipole moment that couples to the electric field of the cavity. We have obtained a charge coupling rate of $g_c \sim 30$ MHz for this system, which is larger than the coupling rate obtained in the first superconducting qubit/cavity experiments in 2004 (6). Strong spin-orbit interactions in InAs couple

the orbital position of the electron to the spin, enabling electrical control of spin and spin state readout via the cavity (10, 11). Limitations of InAs include short spin dephasing times due to nuclear spins. A longer spin dephasing time would make a spin SWAP operation feasible with the cavity based approach.

The motivation for the research effort is to demonstrate spin-cavity coupling in a system that exhibits long spin coherence times. Specifically, we will couple a silicon double quantum dot spin qubit to the microwave cavity. Silicon is known to have a long spin lifetime, ~6 seconds, and spin dephasing times that are at least a factor of 20 larger than in III/V semiconductors. However, the spin-orbit interaction is weaker in silicon. As a result, we will generate artificial spin-orbit coupling by incorporating micromagnets into the quantum dot design. The micromagnets will provide a field gradient that results in a position dependent Zeeman splitting. The slanting field of the micromagnet has been employed by several groups to drive electron spin resonance transitions without the use of a standard ac magnetic field. In these experiments, the ac magnetic field is created by shifting the orbital position of a single electron in the slanting Zeeman field of the micromagnet (12-15). Typical field gradients are on the order of several Gauss per nanometer, leading to a large effective spin-orbit coupling.

3.0 METHODS, ASSUMPTIONS, AND PROCEDURES

The main idea of the proposal is to couple a two-electron spin qubit to a microwave cavity, clearing the way for an architecture that will allow rapid scaling of spin qubit technology. Direct coupling of a spin to the magnetic field of a microwave resonator is on the order of 10 Hz; far too slow to be useful given dephasing and relaxation times (16). It has been proposed to use a combination of electric field coupling and spin-orbit interactions in order to obtain spin-electric coupling (17). My group has explored this approach in InAs nanowires, obtaining a large charge coupling rate of 30 MHz and an estimated spin-coupling strength of 1 MHz. Unfortunately the spin dephasing times are too short in InAs to allow a coherent spin SWAP via the cavity. The success of this approach will require implementation in a system with longer spin dephasing times, such as Si/SiGe. Since spin-orbit is very weak in Si, we will rely on micromagnets to give a spatially dependent Zeeman splitting, which will take the place of the spin-orbit interaction used in our InAs nanowire experiments (15).

There are three main components that create the proposed device: 1) superconducting resonator, 2) double quantum dot, and 3) micromagnet. We wish to improve the fabrication of these three components significantly, which will result in direct gains in the spin-cavity coupling strength.

3.1 Superconducting resonator

The superconducting resonator generates an ac electric field that couples to the dipole moment of the electron trapped in the double quantum dot. There are several important factors to address. First, the resonance frequency of the cavity must be matched to the energy level splitting in the quantum dot, either an orbital or spin transition. This naturally places the resonance frequency in the 5-20 GHz range. Second, the cavity must have a high quality factor, otherwise the photon will escape the cavity before the two-qubit interaction can be completed. Too high of a quality factor can be problematic as well, since it reduces the number of photons that reach the microwave detector.

Incorporation of quantum dots into the resonator leads to additional complications. For coupling to spin qubits, a magnetic field must be applied to lift the Kramer's degeneracy. The magnetic field

required is of order 100 mT, which will drive Al into the normal state. We are therefore restricted to work with Nb resonators, with the external magnetic field applied in the plane of the sample. Thinner superconductors lead to higher critical fields, so the Nb thickness is typically on the order of 50 to 100 nm.

3.2 Double quantum dot

GaAs quantum dots exhibit spin dephasing times on the order of 10 ns. In order to reach the strong coupling regime, where quanta can be coherently transferred from the cavity to the qubit and back, the vacuum Rabi frequency must be larger than the cavity decay rate and the qubit decay rate. Our approach to reach the strong coupling regime is two-fold. We will first increase the electric fields generated by the cavity to create a 100 MHz charge-cavity coupling rate. We will also employ singlet-triplet spin qubits in Si/SiGe, which are known to have coherence times that are at least an order of magnitude longer than those obtained with GaAs spin qubits (18).

3.3 Micromagnet

Effective spin-electric coupling in Si/SiGe spin qubits will be created by incorporating a micromagnet into the quantum dot design (15). The micromagnet results in a spatially varying Zeeman splitting, which has been used by the Tarucha group for single spin control (13). The energy of the spin state will therefore be sensitive to the position of the electron in the quantum dot. The field from the micromagnet must not interfere with the superconducting resonator, otherwise the quality factor will be reduced, or in the worst case, the Nb film will be pushed into the normal state.

3.4 Discussion of other possible spin coupling approaches

The exchange gate allows rapid coupling of adjacent electron spins in semiconductor double quantum dots. Several approaches can be employed to couple spin qubits that are separated by longer distances. We briefly summarize three approaches here.

3.4.1 Direct capacitive interaction

Full control of the Bloch vector in singlet-triplet spin qubits is achieved using magnetic field gradients and the exchange interaction. The exchange interaction is sensitive to gate voltages, allowing rapid electrical control. One approach to coupling spin qubits is based on a capacitive interaction between two adjacent singlet-triplet spin qubits (19). The main idea is that the charge configuration of one of the qubits will influence the exchange energy of the other qubit, leading to a controlled phase rotation (9).

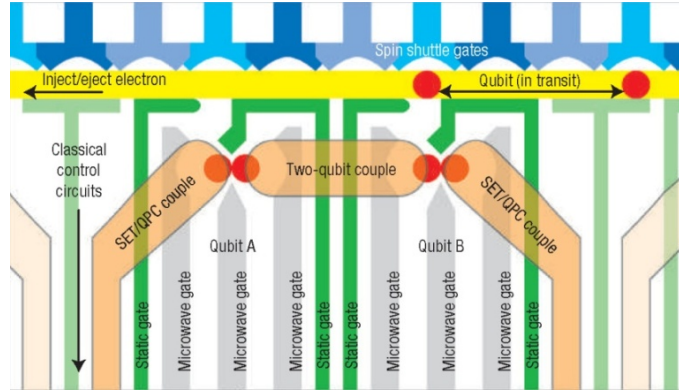


Figure 2. Fault-tolerant spin-based quantum computer architecture proposed by Taylor *et al.* Distant qubits in this proposal are coupled by physically transporting single spins from one double quantum dot to a distant double quantum dot. Adapted from ref. 19.

3.4.2 Spin bus

In theory, quantum information can be transferred along a spin bus consisting of a 1D chain of exchange coupled spins. The idea here is to perform unitary operations on one spin in the chain (which could be one spin in a singlet-triplet qubit). The spin chain allows propagation of information to the other end of the chain, allowing coupling, or transfer of quantum information over longer distances.

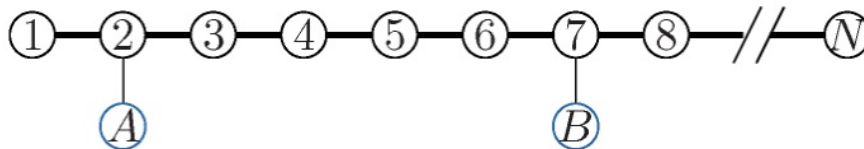


Figure 3. Schematics of two qubits, A and B, weakly attached to nodes $i=2$ and $j=7$ of a chain with N spins. Adapted from ref. 2.

3.4.2 cQED architecture (this project)

cQED allows long range coupling of superconducting qubits and will be extended to spin qubits in this proposal. Strengths of this proposal include: a) long distances- coupling can be achieved between qubits that are separated by ~ 1 cm (set by the wavelength of the microwave field), b) scale- the dimensions of the cavity bus are quite large, allowing a large number of spin qubits to be coupled to a single cavity, c) the microwave cavity acts as a notch-pass filter, eliminating sources of noise away from the resonant frequency of the cavity.

4.0 RESULTS AND DISCUSSION

4.1 Development of high quality factor superconducting resonators on Si/SiGe two-dimensional electron gas substrates

A major effort has been directed at developing a fabrication process for superconducting resonators on wafers containing Si/SiGe two-dimensional electron gases. In earlier published work, InAs nanowire double quantum dots were coupled to high quality factor superconducting resonators (20). However, these resonators were fabricated on undoped high resistivity Si wafers that did not experience the chemical vapor deposition processing required to grow Si/SiGe two-dimensional electron gases.

4.2 Resonator fabrication

The wafer is cleaned in 1:10 buffered oxide etch for 5 minutes to remove the native oxide on the wafer. In sections 4.1.2-4.1.5 we then deposit 50 nm of Al_2O_3 by atomic layer deposition but in sections 4.1.6-4.1.7 we deposit 15 nm instead to accommodate an existing quantum dot recipe. The substrate is then loaded into a sputtering system and the vacuum chamber is pumped down to approximately 3×10^{-8} Torr. A 50 nm thick film of Nb is sputtered at a rate of 0.79 Å/s with the substrate held at room temperature.

Resonators are defined using photolithography. We use S1818 photoresist and a contact aligner to achieve micron accuracy. The Nb is then etched in a RIE. The Nb etch is performed with an SF_4 flow rate of 50 sccm and O_2 flow rate of 5 sccm. An RF field of strength of 250 Watts is used to generate the plasma, while a 50 Watt field drives the ions into the substrate. The layer of Al_2O_3 serves as an etch stop to prevent damage to the substrate. After the RIE, the Al_2O_3 is etched using a 2 minute wet etch in 1:10 buffered oxide etch. In section 4.6 thin Ti/Au gold contacts of thickness 3 nm/10.5 nm are defined using electron beam lithography on PMMA A4 electron beam resist. In section 4.7, thick layered Ti/Au gates are added using photolithography with layered LOR5A and S1818, evaporating 5 nm/100 nm of Ti/Au, and lifting off the Ti/Au in Remover PG.

4.2.1 Testing of Nb resonators on low-resistivity Si with Si/SiGe heterostructures

Substrates: Samples were fabricated on Si substrates with 100 orientation and resistivity 10 ohm-cm with a $\text{Si}/\text{Si}_{0.7}\text{Ge}_{0.3}$ heterostructure grown on top.

Characterization at 4.2 K: We measured one resonator on this substrate at 4.2 K in a liquid helium bath. The resonator had a designed center frequency of 10 GHz and designed Q of 25,000. Figure 4(a) shows transmission through the resonator versus frequency at 4.2K. The measured Q at 4.2K was 440, limited both by thermal fluctuation as well as the low resistivity of the Si substrate, as discussed in section 4.4.

Characterization at 15mK: The sample was then measured at $T = 15$ mK in a dilution refrigerator. Figure 4(b) shows transmission through the resonator versus frequency at 15 mK. The resonator had a resonant frequency of 10.33 GHz and quality factor of 3,160.

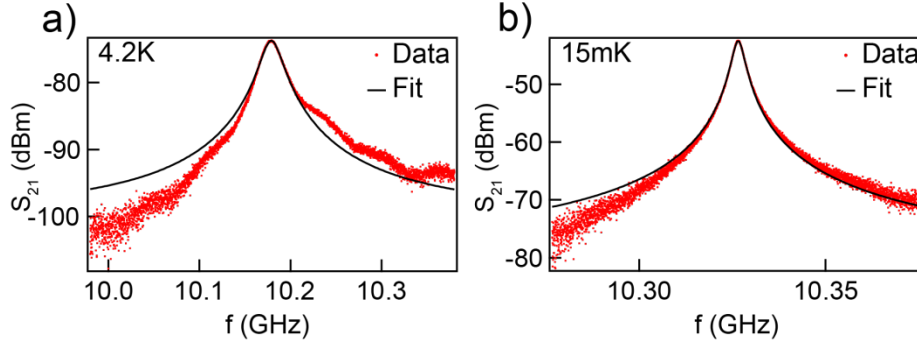


Figure 4 a) Transmission versus frequency for the resonator on low-resistivity Si with a Si/SiGe heterostructure at 4.2 K. The measured Q at 4.2 K was 440. b) Transmission versus frequency for the same resonator at 15 mK. The measured Q at 15 mK was 3,160.

4.2.2 Testing of Nb resonators on low-resistivity Si with Si/SiGe heterostructure subject to Ar ion destruction

The low quality factors in Fig. 4 suggests that the substrate or Si/SiGe relaxed buffer is limiting the ultimate quality factor. To render the substrate insulating, we impacted the sample with high energy Ar ions using a process called ion isolation. The goal was to increase the resistivity of the substrate and relaxed buffer, therefore increasing the quality factor of the resonators.

Substrates: Samples were fabricated on Si substrates with 100 orientation and resistivity 10 ohm-cm with a Si/SiGe heterostructure grown on top which was then implanted with Ar atoms to destroy the Si/SiGe heterostructure.

Characterization at 4.2 K: We measured one resonator on this substrate at 4.2 K in a liquid helium bath. The resonator had a designed center frequency of 10 GHz and designed Q of 25,000. Figure 2 shows transmission through the resonator versus frequency at 4.2 K. The measured Q at 4.2 K was 235, limited both by thermal fluctuation as well as the low resistivity of the Si substrate. The dramatic lowering of the Q suggests that ion isolation introduces dissipative defects. This approach is no longer being pursued.

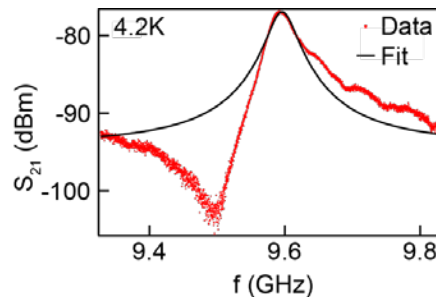


Figure 5 Transmission versus frequency for the resonator on low-resistivity Si and Ar destructed SiGe heterostructure at 4.2 K. The measured Q at 4.2 K was 235.

4.3 Simulations to determine the effect of the substrate resistivity on the resonator quality factor

In order to determine the cause of the low quality factors of the resonators on low-resistivity Si with a Si/SiGe heterostructure, electric field simulations were carried out to determine the percentage of the resonator's electric field in each portion of the substrate. It was found that 30% of the field resides in the 675 μm thick low-resistivity Si substrate on which the Si/SiGe heterostructure is grown, 55% resides in the 3 μm thick SiGe relaxed buffer (a linear gradient from with increasing Ge concentration from Si to $\text{Si}_{0.7}\text{Ge}_{0.3}$) and 300 nm of $\text{Si}_{0.7}\text{Ge}_{0.3}$ grown above the relaxed buffer, and 15% resides in the remaining Si/SiGe heterostructure (see Figure 6). The significant portion of the field that resides in the low-resistivity Si as well as the fact that the loss tangent of a material is inversely proportional to its resistivity motivated us to obtain higher-resistivity Si on which Si/SiGe heterostructures could be grown.

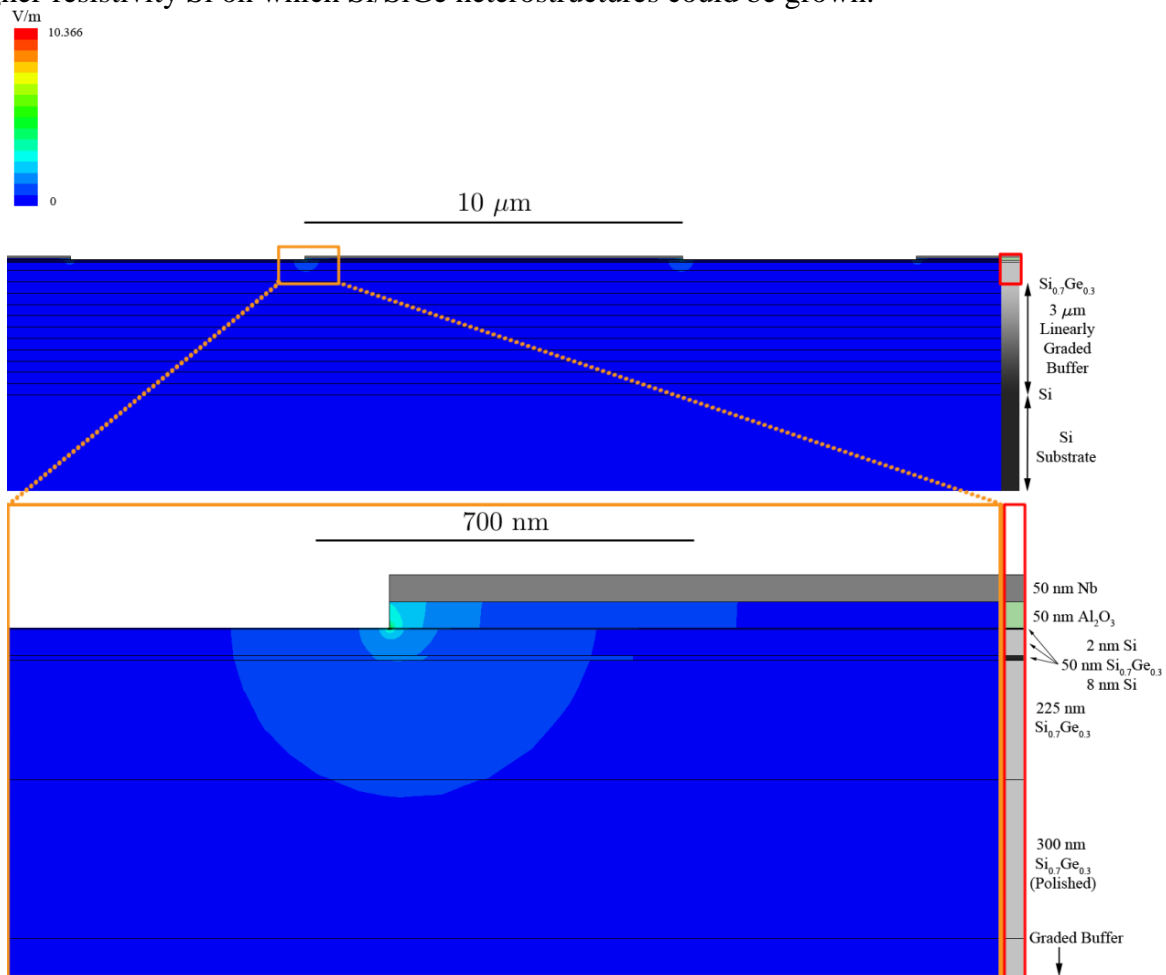


Figure 6 Electric field simulation of a resonator that shows the distribution of the electric field from the resonator center pin in the different layers of the substrate.

4.4 Testing of Nb resonators on high-resistivity Si

Substrates: Next, samples were fabricated on high resistivity Si substrates with 100 orientation and resistivity >5000 ohm-cm.

Fabrication Results: We first characterized a resonator with a design Q of 50,000 and a design resonance frequency of 11.1 GHz. The resonator design dimensions are a 10 micron center pin and a 5.8 micron vacuum gap. Figure 7 shows an optical image of the resonator center pin. The measured dimensions are 10.4 microns for the center pin width and 5.8 microns for the vacuum gap. Figure 8(a) shows the design of the input and output coupling capacitors and the optical image in Figure 8(b) shows the measured dimensions. The measured dimensions closely follow the design and represent the limit of contact optical lithography. The resulting capacitance is calculated to be 0.8 fF, giving an expected Q of 90,000.

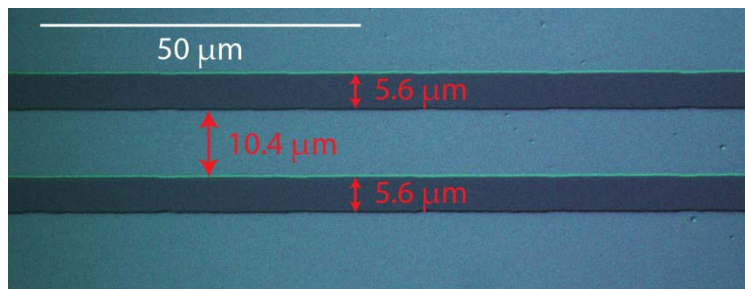


Figure 7 Optical micrograph of the resonator's center pin.

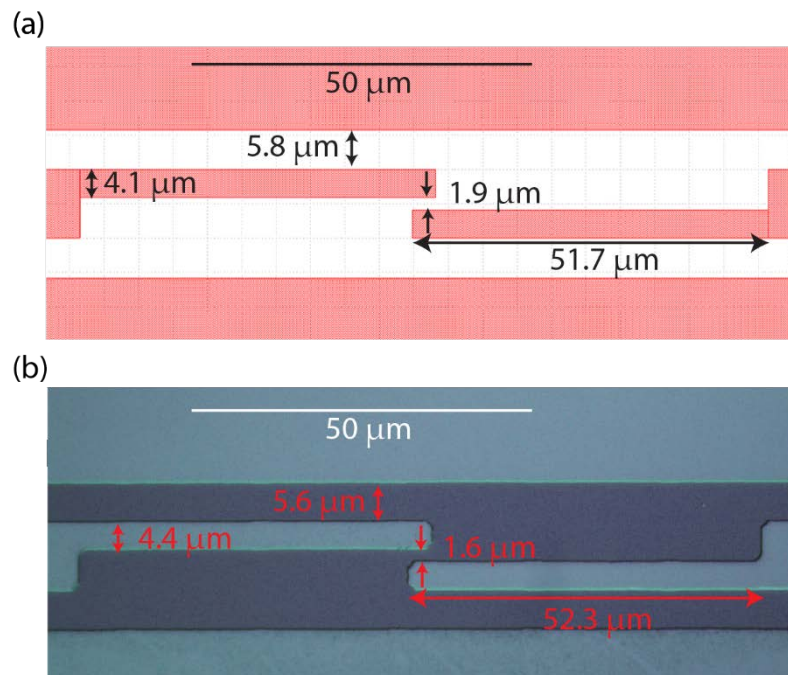


Figure 8 a) Design of the coupling capacitor. Critical design dimensions are indicated. b) Optical micrograph of the fabricated device. Measured dimensions agree well with the design parameters.

Characterization at 4.2 K: We measured two resonators on bare high-resistivity Si at 4.2 K in a liquid helium bath. Design 1 has a design Q of 270,000 (based solely on the coupling capacitance and resonance frequency of the design) and a design center frequency of 9.5 GHz. Design 2 has an expected Q of 90,000 (based on the measured capacitor dimensions) and a design center frequency of 11.1 GHz. Figure 9 shows transmission through the resonator versus frequency at 4.2 K for both designs. In both cases the Q was limited by thermal fluctuation to approximately 1100.

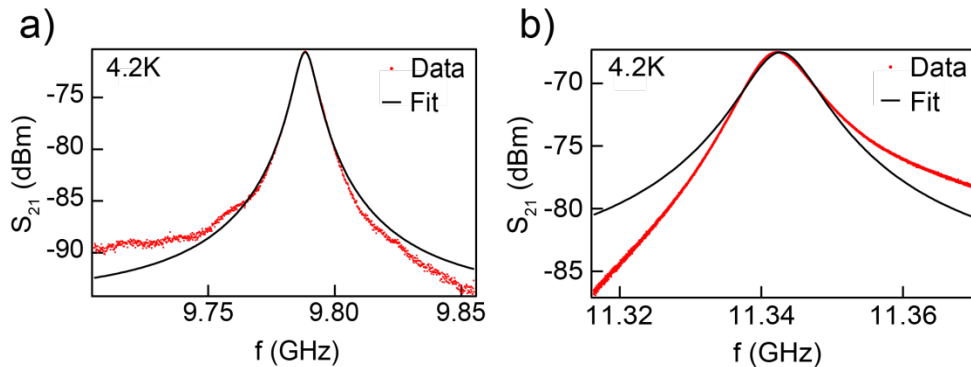


Figure 9 a) Transmission versus frequency for Design 1 on bare high-resistivity Si at 4.2 K. The measured Q at 4.2 K was 1,161. b) Transmission versus frequency for Design 2 on bare high-resistivity Si at 4.2 K. The measured Q at 4.2 K was 1,109.

Characterization at 8 mK: The samples were then measured at $T = 8$ mK in a dilution refrigerator. Figure 10 shows transmission through the resonator versus frequency at 8 mK for both designs. Design 1 had a resonance frequency of 9.86 GHz and a Q of approximately 101,000 and Design 2 had a resonance frequency of 11.42 GHz and a Q of approximately 73,000. We note that these quality factors are lower than designed, but can be explained as substrate losses.

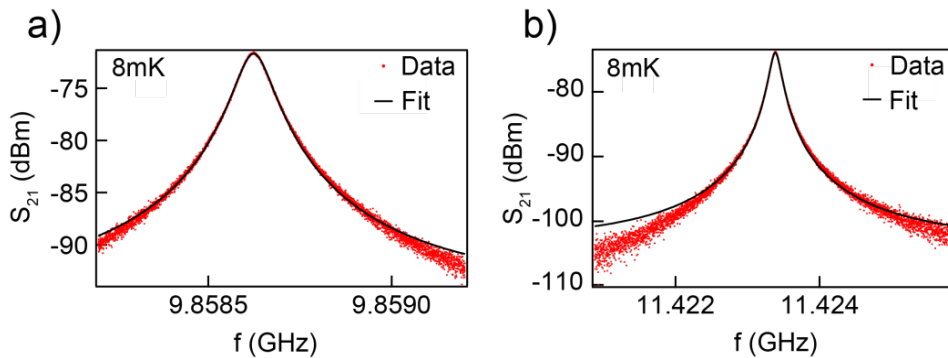


Figure 10 a) Transmission versus frequency for Design 1 on bare high-resistivity Si at 8 mK. The measured Q at 8 mK was 100,836. b) Transmission versus frequency for Design 2 on bare high-resistivity Si at 8 mK. The measured Q at 8 mK was 73,316.

These data indicate that there is no problem reaching the target quality factor of 10,000 on bare high resistivity Si substrates.

4.5 Testing of Nb resonators on high-resistivity Si with a SiGe relaxed buffer substrate

The high quality factors demonstrated in section 4.4 are encouraging. We next proceeded to have SiGe relaxed buffers grown on the high resistivity Si wafers. Resonators were then fabricated and tested.

Substrates: Samples were fabricated on high resistivity Si substrates with 100 orientation and resistivity >5000 ohm-cm that has a 3 micron thick SiGe relaxed buffer that is linearly graded in Ge concentration from 0% to 30% and a 300nm thick layer of $\text{Si}_{0.7}\text{Ge}_{0.3}$ on top of that.

Characterization at 4.2 K: We characterized two resonators on this substrate at 4.2 K in a liquid helium bath. Design 1 has a target Q of 125,000 and a target center frequency of 7 GHz. Design 2 has a target Q of 60,000 and a target center frequency of 8 GHz. Design 3 has a target Q of 70,000 and a target center frequency of 11 GHz. Figure 11 shows transmission through the resonators versus frequency at 4.2 K for all designs. As before, the quality factors are limited by the temperature.

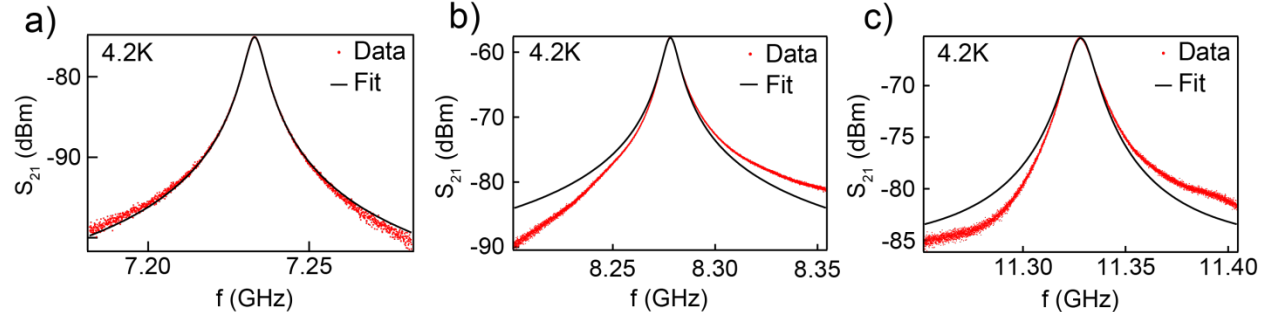


Figure 11 a) Transmission versus frequency for Design 1 on high-resistivity Si with a SiGe relaxed buffer at 4.2 K. The measured Q at 4.2 K was 1,260. b) Transmission versus frequency for Design 2 on high-resistivity Si with a SiGe relaxed buffer at 4.2 K. The measured Q at 4.2 K was 1,160. c) Transmission versus frequency for Design 3 on high-resistivity Si with a SiGe relaxed buffer at 4.2 K. The measured Q at 4.2 K was 866.

Characterization at 10 mK: Designs 1 and 3 were then measured at 10 mK in a dilution refrigerator. Figure 12 shows transmission through the resonator versus frequency at 10 mK for both designs. Design 1 had a resonance frequency of 7.296 GHz and a Q of approximately 131,000 and Design 3 had a resonance frequency of 11.419 GHz and a Q of approximately 54,000.

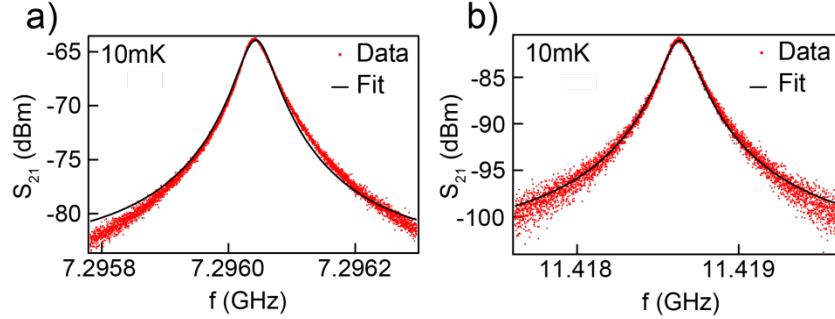


Figure 12 a) Transmission versus frequency for Design 1 on high-resistivity Si with a SiGe relaxed buffer at 10 mK. The measured Q at 10 mK was 131,000. b) Transmission versus frequency for Design 3 on high-resistivity Si with a SiGe relaxed buffer at 10 mK. The measured Q at 10 mK was 54,000.

Similar to section 4.4, these data indicate that there is no problem reaching the target quality factor of 10,000 on high resistivity Si substrates containing SiGe relaxed buffer layers.

4.6 Testing of Nb resonators on high-resistivity Si with Si_{0.7}Ge_{0.3} relaxed buffer layers and a dc contact for electrical coupling to a triple quantum dot

Realistic device architectures will require the center pin of the resonator to be contacted to the source or drain contact of the quantum dot. This kind of device architecture, first developed at Princeton by Petersson *et al.*, maximizes the electric field at the double quantum dot (20). Working towards a final device prototype, we fabricated increasingly complex resonators in an effort to maintain high quality factors.

Substrates: Samples were fabricated on high resistivity Si substrates with 100 orientation and resistivity >5000 ohm-cm that has a 3 micron thick SiGe relaxed buffer that is linearly graded in Ge concentration from 0% to 30% and a 300 nm thick layer of Si_{0.7}Ge_{0.3} on top of that. Layered Ti/Au contacts of thickness 3 nm/10.5 nm are fabricated underneath the resonator center pin and in gaps in the ground plane to provide DC connections between various metal layers.

Characterization at 4.2 K: We characterized 5 resonators of this kind at 4.2 K in a liquid helium bath, all of which had a target center frequency of 7.5 GHz. Three of the resonators are conventional coplanar waveguide resonators modified to allow capacitive coupling to triple quantum dots at either end of the resonator. These designs, which we will call A0, A1, and A2, have target quality factors of 15,000, 30,000, and 20,000, respectively. Figure 13 shows transmission as a function of frequency at 4.2 K for these three resonators. The other two resonators have a spiral inductor connected to their midpoints so that DC bias can be applied to the resonator center pin. These designs, which we shall call B0 and B1, have target Qs of 15,000 and 30,000, respectively. These two designs were tested at 4.2 K with the spiral inductor both floating and connected to ground. Figure 14 shows transmission as a function of frequency at 4.2 K for all four of these resonator configurations. The Q of all of these devices and configurations at 4.2K was limited to approximately 1,500 by thermal fluctuations. Whether or not the spiral inductors of B0 and B1 were grounded did not appear to significantly affect the quality factors of those resonators.

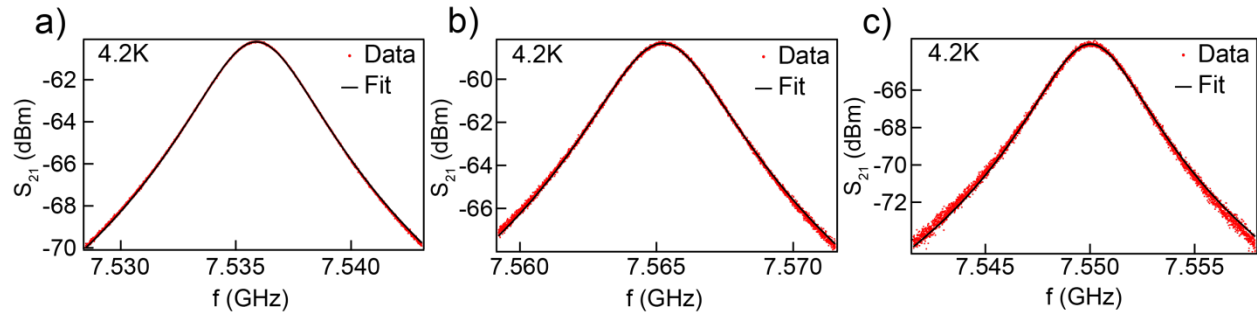


Figure 13 a) Transmission versus frequency for design A0 at 4.2 K. Its measured Q at 4.2 K was 1,490. b) Transmission versus frequency for design A1 at 4.2 K. Its measured Q at 4.2 K was 1,650. c) Transmission versus frequency for design A2 at 4.2 K. Its measured Q at 4.2 K was 1,570.

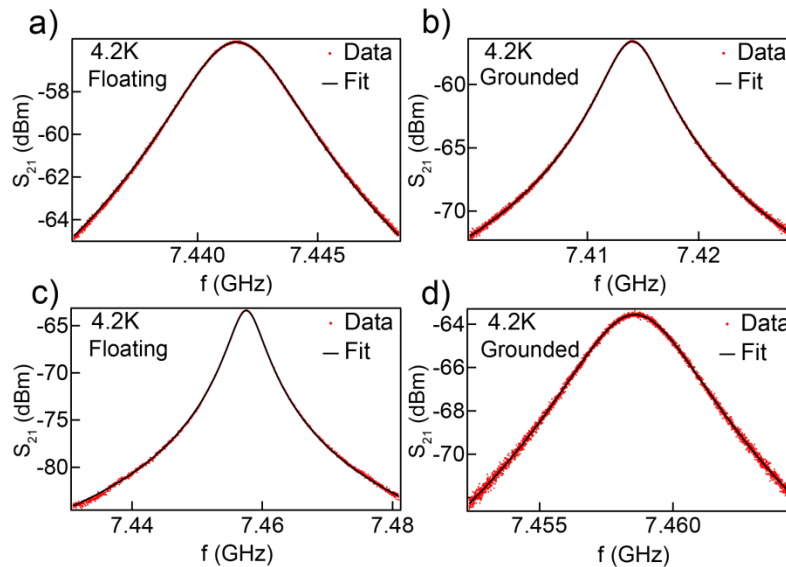


Figure 14 a) Transmission versus frequency for design B0 at 4.2 K with its spiral inductor floating. The measured Q of this configuration was 1,480. b) Transmission versus frequency for design B0 at 4.2 K with its spiral inductor connected to ground. The measured Q of this configuration was 1,480. c) Transmission versus frequency for design B1 at 4.2 K with its spiral inductor floating. The measured Q of this configuration was 1,570. d) Transmission versus frequency for design B1 at 4.2 K with its spiral inductor connected to ground. The measured Q of this configuration was 1,510.

Characterization at 10 mK: The A0 design was then measured at $T = 10\text{mK}$ in a dilution refrigerator. Figure 12 shows transmission through the resonator versus frequency at 10 mK. Its measured resonance frequency and Q at 10 mK were 7.568 GHz and 16,500.

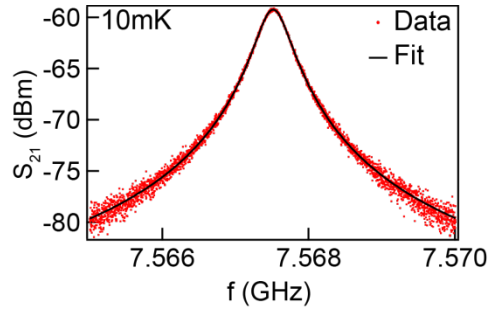


Figure 15 Transmission versus frequency for design A0 at 10 mK. The measured Q of this device at 10 mK was 16,500.

4.7 Testing of Nb resonators on high-resistivity Si with Si_{0.7}Ge_{0.3} relaxed buffer with a gold contact for coupling to triple quantum dot and gold gates

Substrates: Samples were fabricated on high resistivity Si substrates with 100 orientation and resistivity >5000 ohm-cm that has a 3 micron thick SiGe relaxed buffer that is linearly graded in Ge concentration from 0% to 30% and a 300 nm thick layer of Si_{0.7}Ge_{0.3} on top of that. Layered Ti/Au contacts of thickness 3 nm/10.5 nm are fabricated underneath the resonator center pin and in gaps in the ground plane to provide DC connections between various metal layers. In addition, layered Ti/Au gates of thickness 5 nm/100 nm are deposited in the same ground plane gap as the Ti/Au contacts to mimic the metallic architecture necessary to support triple quantum dots.

Characterization at 4.2 K: The A0, A1, and A2 designs from the prior section had gold gates added to them and were characterized at 4.2 K in a liquid helium bath. The Q at 4.2 K of all three designs was lowered to approximately 1,000 by the addition of the gold gates. Figure 16 shows transmission versus frequency at 4.2 K for these resonators.

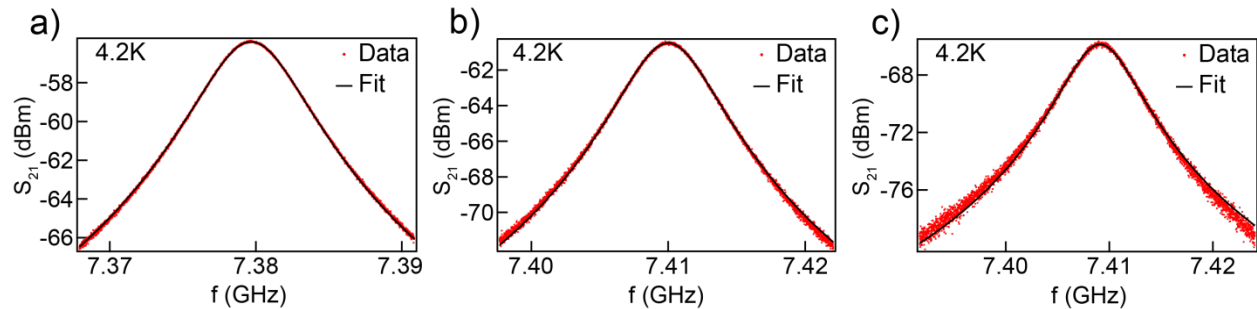


Figure 16 a) Transmission versus frequency at 4.2 K for design A0 with thick gold gates added. The measured Q at 4.2 K of this device was 1,020. b) Transmission versus frequency at 4.2 K for design A1 with thick gold gates added. The measured Q at 4.2 K of this device was 1,070. c) Transmission versus frequency at 4.2 K for design A2 with thick gold gates added. The measured Q at 4.2 K of this device was 1,030.

Characterization at 10 mK: The A0 design with thick gold gates added was then measured at $T = 10$ mK in a dilution refrigerator. Figure 17 shows transmission through the resonator versus

frequency at 10 mK. Its measured resonance frequency and Q at 10 mK were 7.448 GHz and 10,700.

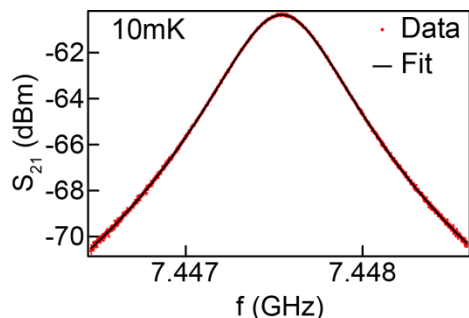


Figure 17: Transmission versus frequency at 10 mK for design A0 with thick gold gates added. The measured Q of this device at 10 mK was 10,700.

The lower quality factor of this device compared to the identical device without thick gold gates suggests that these gates limit the Q of the device. However, the quality factor of 10,700 measured here is significantly higher than has been seen in similar devices and should serve initial semiconductor circuit QED experiments well.

In order to gauge how this resonator will perform when coupled to quantum dots, the line attenuation leading to and from the resonator in the dilution refrigerator was estimated, allowing us to approximate the number of photons present in the cavity for a given resonator drive power. Figure 18 shows the Q of this A0 device with thick gold gates as a function of approximate number of photons in the cavity. Even when there are fewer than 10 photons in the cavity, the quality factor of the resonator is still comparable to its quality factor at higher drive powers, which is promising for the prospect of performing circuit QED experiments with these devices like those done with superconducting qubits and InAs nanowire quantum dots.

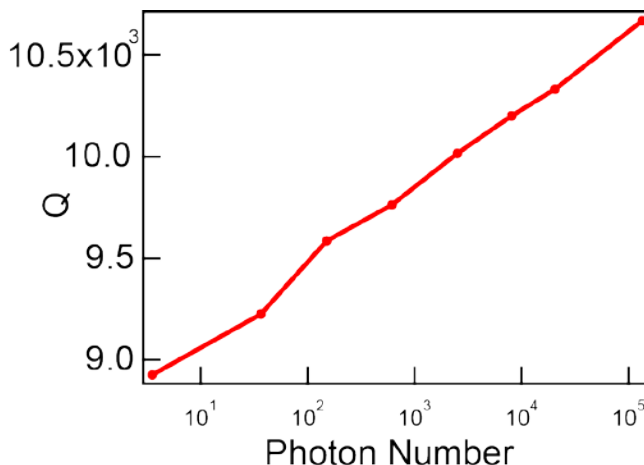


Figure 18: Quality factor versus approximate number of photons in the cavity for design A0 with thick gold gates.

4.8 Summary of resonator optimizations and possible further optimizations

The resonators in sections 4.3.1 and 4.3.2 were clearly performance-limited in some way. The simulations in section 4.4 suggested that the Q -limiting factor could have been the low-resistivity Si on which the Si/SiGe heterostructure was grown. High quality factor resonators were then demonstrated on bare high-resistivity Si and then on high-resistivity Si with a SiGe relaxed buffer grown on top. These results, combined with the result from the field simulations in section 4.3 that 85% of the electric field from the resonator resides in the Si substrate and relaxed buffer, gave us confidence that the high-resistivity Si had remedied the cause of the low quality factors seen in sections 4.2.1 and 4.2.2. In sections 4.6 and 4.7 it was shown that a resonator architecture capable of supporting triple quantum dot integration allowed for high quality factors, but that the gold used for much of the gate architecture is likely limiting the quality factor of these resonators.

It remains to be tested whether accumulation of two-dimensional electron gas under the resonator center pin of the B0 and B1 devices discussed in sections 4.6 and 4.7 has a deleterious effect on the resonator quality factor. We intend to test this in the very near future. In terms of long-term considerations, if quality factors must be further optimized, determining whether the replacement of gold with a superconducting metal such as Niobium leads to higher quality factors will likely be a priority.

4.9 Testing of Hall bars on low-resistivity Si with a Si/SiGe heterostructure

Substrates: Samples were fabricated on Si substrates with 100 orientation and resistivity 10 ohm-cm with a Si/SiGe heterostructure grown on top.

Two Hall bar samples were fabricated in order to test the effects of the resonator fabrication process on the two-dimensional electron gas (2DEG) in the Si/SiGe heterostructure: one using a standard Hall bar recipe and one subjected to Al₂O₃ and Nb deposition and etching (described in the resonator fabrication paragraph at the beginning of this report) before undergoing the same Hall bar recipe as the first sample. These samples are referenced as “unprocessed” and “processed” respectively.

Characterization at 300 mK: Both samples were cooled to approximately 300 mK in a ³He cryostat and measured in the presence of a magnetic field $B = 200$ mT. Standard Hall measurements were then taken and used to calculate the 2DEG mobility, μ , and electron density, n , as a function of applied top gate voltage for both samples. The results of the measurement are compiled in Figure 19 and demonstrate that the 2DEG characteristics are unaffected by the resonator processing, which should allow quantum dots and resonators to be successfully fabricated on the same chip.

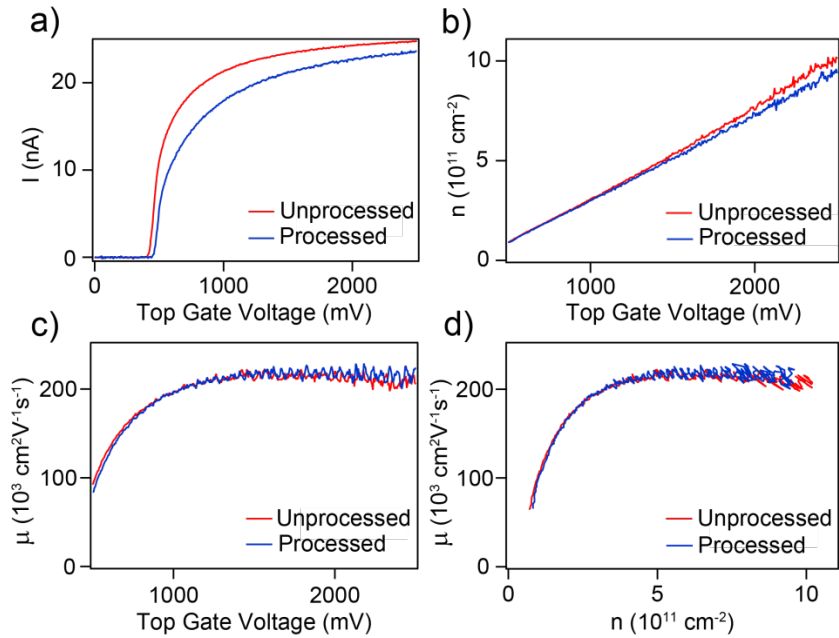


Figure 19 All data taken at approximately 300 mK. a) Source-drain current versus top gate voltage for both the unprocessed and processed samples. b) Electron density versus top gate voltage for both samples. c) Mobility versus top gate voltage for both samples. d) Mobility versus electron density for both samples. The similarity between the two data sets shows that the resonator fabrication steps do not harm the 2DEG.

4.10 Development of accumulation only gate architecture

We developed an overlapping gate architecture for accumulation mode quantum dots on Si/SiGe heterostructures. The device is shown in Fig. 20. It consists of a pair of double dots that could be reconfigured to make a single dot charge sensor on one side and a double dot on the other side of the device.

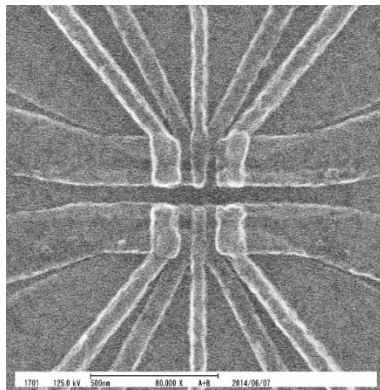


Figure 20 An SEM image of an “accumulation only” double quantum dot. For the data presented in Fig. 20, the bottom double dot was tuned a single dot to sense the top double dot.

This was also the first device tested with dot widths of 80 nm and tunnel barrier widths of 20 nm. Although it might be possible to make smaller tunnel barriers with our current e-beam process, the data from the device looks like 20 nm barriers might be sufficient to prevent dots from forming under the barrier gates.

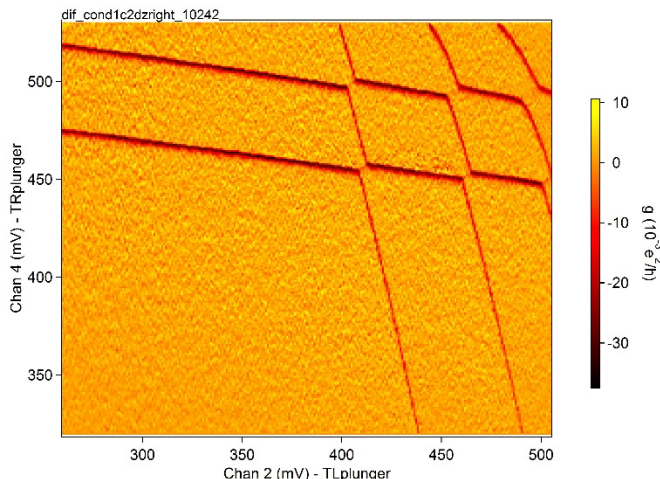


Figure 21 Numerical derivative of the charge sensor conductance as a function of the left and right plunger voltages showing the charge stability diagram of the upper double dot and the emptying of all electrons from both dots (no charge transitions in the lower left of the plot). The sensor dot voltage was linearly adjusted to maintain constant charge sensitivity while adjusting the left and right plunger voltages.

5.0 CONCLUSIONS

We showed that it is possible to achieve high quality factor resonators on Si/SiGe substrates at frequencies exceeding 10 GHz. In addition, through this research program, we were able to develop a new style of quantum dot device architecture that operates in accumulation mode. These devices are easily capable of reaching the few-electron regime. Due to significant challenges associated with the growth of high quality Si/SiGe two-dimensional electron gas samples, we were unable to measure the coupling between the double quantum dot and the microwave cavity. However, devices are currently fabricated to allow such tests and we anticipate several publications to result from this work in the next 12 month period.

6.0 REFERENCES

1. M. Friesen, A. Biswas, X. Hu, D. Lidar, Efficient multiqubit entanglement via a spin bus. *Phys. Rev. Lett.* **98**, 230503 (2007).
2. S. Oh, M. Friesen, X. Hu, Even-odd effects of Heisenberg chains on long-range interaction and entanglement. *Phys. Rev. B* **82**, 140403 (2010).
3. S. Oh *et al.*, Heisenberg spin bus as a robust transmission line for quantum-state transfer. *Phys. Rev. A* **84**, 022330 (2011).
4. A. Blais, R. S. Huang, A. Wallraff, S. M. Girvin, R. J. Schoelkopf, Cavity quantum electrodynamics for superconducting electrical circuits: An architecture for quantum computation. *Phys. Rev. A* **69**, 062320 (2004).
5. M. D. Reed *et al.*, Realization of three-qubit quantum error correction with superconducting circuits. *Nature* **482**, 382 (2012).
6. A. Wallraff *et al.*, Strong coupling of a single photon to a superconducting qubit using circuit quantum electrodynamics. *Nature* **431**, 162 (2004).
7. M. A. Sillanpää, J. I. Park, R. W. Simmonds, Coherent quantum state storage and transfer between two phase qubits via a resonant cavity. *Nature* **449**, 438 (2007).
8. B. R. Johnson *et al.*, Quantum non-demolition detection of single microwave photons in a circuit. *Nature Phys.* **6**, 663 (2010).
9. J. R. Petta *et al.*, Coherent manipulation of coupled electron spins in semiconductor quantum dots. *Science* **309**, 2180 (2005).
10. S. Nadj-Perge, S. M. Frolov, E. Bakkers, L. P. Kouwenhoven, Spin-orbit qubit in a semiconductor nanowire. *Nature* **468**, 1084 (2010).
11. M. D. Schroer, K. D. Petersson, M. Jung, J. R. Petta, Field tuning the g factor in InAs nanowire double quantum dots. *Phys. Rev. Lett.* **107**, 176811 (2011).
12. T. Obata *et al.*, Coherent manipulation of individual electron spin in a double quantum dot integrated with a micromagnet. *Phys. Rev. B* **81**, 085317 (2010).
13. M. Pioro-Ladriere *et al.*, Electrically driven single-electron spin resonance in a slanting Zeeman field. *Nature Phys.* **4**, 776 (2008).
14. M. Pioro-Ladriere, Y. Tokura, T. Obata, T. Kubo, S. Tarucha, Micromagnets for coherent control of spin-charge qubit in lateral quantum dots. *Appl. Phys. Lett.* **90**, 024105 (2007).
15. Y. Tokura, W. G. van der Wiel, T. Obata, S. Tarucha, Coherent single electron spin control in a slanting Zeeman field. *Phys. Rev. Lett.* **96**, 047202 (2006).
16. Y. Kubo *et al.*, Strong coupling of a spin ensemble to a superconducting resonator. *Phys. Rev. Lett.* **105**, 140502 (2010).
17. M. Trif, V. N. Golovach, D. Loss, Spin dynamics in InAs nanowire quantum dots coupled to a transmission line. *Phys. Rev. B* **77**, 045434 (2008).
18. B. M. Maune *et al.*, Coherent singlet-triplet oscillations in a silicon-based double quantum dot. *Nature* **481**, 344 (2012).
19. J. M. Taylor *et al.*, Fault-tolerant architecture for quantum computation using electrically controlled semiconductor spins. *Nature Phys.* **1**, 177 (2005).
20. K. D. Petersson *et al.*, Circuit quantum electrodynamics with a spin qubit. *Nature* **490**, 380 (2012).

7.0 LIST OF SYMBOLS, ABBREVIATIONS, AND ACRONYMS

2DEG:	2 dimensional electron gas
DQD:	Double quantum dot
Q:	Quality factor
SIMS:	Secondary ion mass spectroscopy